Digital Color Images Ownership Authentication via Efficient and Robust Watermarking in a Hybrid Domain

Manuel CEDILLO-HERNANDEZ [1], Antonio CEDILLO-HERNANDEZ [1],
Francisco GARCIA-UGALDE [2], Mariko NAKANO-MIYATAKE [1], Hector PEREZ-MEANA [1]

[1] Instituto Politecnico Nacional SEPI ESIME Culhuacan, Avenida Santa Ana 1000, San Francisco Culhuacan Coyoacan, Ciudad de Mexico, Mexico
[2] Universidad Nacional Autonoma de Mexico, Facultad de Ingenieria, Avenida Universidad 3000 Ciudad Universitaria Coyoacan, Ciudad de Mexico, Mexico

{ mcedilloh, mnakano, hmperezm }@ipn.mx, antoniochz@hotmail.com, fgarciau@unam.mx

Submitted November 14, 2016 / Accepted March 21, 2017

Abstract. *We propose an efficient, imperceptible and highly robust digital watermarking scheme applied to color images for ownership authentication purposes. A hybrid domain for embedding the same watermark is used in this algorithm, which is composed by a couple of watermarking techniques based on spread spectrum and frequency domain. The visual quality is measured by three metrics called Peak Signal to Noise Ratio (PSNR), Structural Similarity Index (SSIM) and Visual Information Fidelity (VIF). The difference color between the original and watermarked image is computed using the Normalized Color Difference (NCD) measure. Experimentation shows that the proposed method provides high robustness against several geometric distortions including large image cropping, removal attacks, image replacement and affine transformation; signal processing operations including several image filtering, JPEG lossy compression, visual watermark added and noisy image, as well as combined distortions between all of them. Also, we present a comparison with some previously published methods which reported outstanding results and have a similar purpose as our proposal, i.e. they are focused in robust watermarking.*

Keywords

Robust digital watermarking; ownership authentication, spread spectrum, discrete Fourier transform, discrete Contourlet transform

1. Introduction

During the recent years, digital multimedia technologies associated mainly with image, video and audio, are widely consumed by the end users within personal computers and mobile devices through networks, which is a common practice that growing dramatically. This practice allows that digital multimedia data may be easily edited and/or re-distributed without any control type. This behavior requires the necessity of developing efficient tools to solve the problems associated with the infringing of the intellectual property of the multimedia's owner. In the context of digital images, watermarking is considered as a suitable solution for ownership authentication purposes. In this, commonly a small signal called "watermark" is embedded using the information from the spatial or frequency domain of the image, without affecting their visual quality and at the same time it can be detected using a detection algorithm [1], [2]. According to the different applications and requirements, digital image watermarking is classified into two types: visible and invisible. In the invisible context, watermarking is classified into two types: fragile and robust as well. Fragile watermarking modality is used for content protection, authentication, and detection tamper applications while the robust watermarking is used for copyright protection and ownership authentication. Thus, in robust watermarking, according to the detection procedure, the methods are classified into two types: blind and non-blind. In blind watermarking, the original image is not needed to detect the presence of the watermark signal while into the non-blind watermarking the original image is required. In robust watermarking with blind detection, the synchronization loss between embedding-detection stages commonly causes watermark detection errors. Geometric operations such as cropping, removal, rotation, scaling or affine transformation are the principal reasons of this des-synchronization. In the literature, several works are related to robust image watermarking with geometric invariance feature [3–7]. These plans show robustness against rotation and scaling geometric distortions as well as against signal processing operations such as filtering, JPEG compression and among others; because these methods embed the watermark into invariant geometric domains, however, may be typically weak to cropping and removal attacks, affine transformations, and other aggressive distortions. Additionally, while several watermarking algorithms have been proposed to watermark gray-scale images [3–7], until nowadays only a few have been designed specifically for color images [8]. The use of color information has become an essential property to steganography and watermarking of image and video [8], [9]. In this respect, several robust color image watermarking methods have been proposed in the literature, and some of them are based on the frequency domain transform [10], [11], [12], spatial domain [13], [14], histogram modification [15], [16], [17] and Singular Value Decomposition (SVD) [18], [19]. In a particular way, the discrete Contourlet Transform (CT) has been used in the literature as a frequency alternative domain to develop robust color watermarking methods [20], [21]. In general terms, CT has been developed as an accurate bi-dimensional representation that can efficiently represent images containing contours and textures, the CT can capture the directional edges superior to wavelets [22].

In this respect, authors in [20] proposed a robust color watermarking method based on Support Vector Regression (SVR) and Non-Subsampled Contourlet Transform (NSCT), together with an image normalization procedure, to obtain geometric invariance against general affine transformation. Here, the color image is decomposed into three RGB color model components and a region of interest is obtained from the normalized components using the invariant centroid theory. Then, the NSCT is performed on the G channel of the important region. Finally, the watermark is embedded into the color original image by modifying the low-frequency NSCT coefficients, in which a Human Visual System (HVS)-based masking is used to control the watermark embedding strength. According to the high correlation among different channels of the color image, the digital watermark can be recovered using the SVR technique. This algorithm presents robustness against several geometric and signal processing distortions, including cropping attacks. However, the method presents an important drawback: high computation time is needed for SVR training, performing NSCT as well as image normalization process.

Meanwhile, authors in [21] present a blind and highly robust color watermarking scheme method by combining of information from spatial and frequency domain. The watermark signal is generated for each channel RGB of the color image by extracting spatial domain features using gray level co-occurrence matrix as well as a unique identification number. The watermark is embedded in Principal Component Analysis (PCA) less correlated between the low and high frequency of the CT sub-bands to preserve the perceptual quality of the image. This algorithm presents high imperceptibility and at same time robustness against several geometric and signal processing distortions, including cropping attacks and combined distortions; however, the algorithm is not robust against affine general transformation.

To boost the robustness without diminishing the imperceptibility, a very auspicious research direction consists in developing hybrid watermarking algorithms. These algorithms may combine, e.g., the frequency and color image information in conjunction with a geometric correction procedure [20], or the frequency and color image information in conjunction with a frequency analysis procedure [21]. In this context, our paper proposes a highly robust digital watermarking applied to color images for ownership authentication purposes. A hybrid domain for embedding the same watermark is used in this algorithm, which is composed by a pair of watermarking algorithms. In the first one, the luminance channel is used to embed the watermark into the spectrum of the middle frequencies of the Discrete Fourier Transform (DFT) via Direct Sequence Code Division Multiple Access (DS-CDMA). In the second one, the chrominance blue-difference channel is used to embed the watermark into the Contourlet Transform (CT) domain coefficients using an Improved Spread Spectrum (ISS) method. The quality of the watermarked image is measured using the following three well-known indices Peak Signal to Noise Ratio (PSNR), Structural Similarity Index (SSIM) and Visual Information Fidelity (VIF). The difference color between the original and watermarked image is computed using the Normalized Color Difference (NCD) measure. Experimentation shows that the proposed method provides high robustness against several geometric distortions including image cropping, removal attacks, image replacement and affine transformation; signal processing operations including several image filtering, JPEG lossy compression, visual watermark added and noisy image, as well as combined distortions. Also, we present a comparison with some previously published methods which reported outstanding results and have a similar purpose as our proposal, i.e. they are focused in robust watermarking.

The rest of the paper is organized as follows: Section 2 describes the embedding and detection process of the proposed algorithm, and experimental results including comparison with previously reported watermarking algorithms are presented in Sec. 3. Finally, Sec. 4 concludes this work.

2. Proposed Method

The proposed watermarking method consists of the embedding and detection process, which are explained in detail as follows.

2.1 Discrete Fourier Transform Embedding Process

Embedding process is carried out through two stages: the first one operates on DFT domain and the second one on CT domain, respectively. Moreover, the embedding algorithm is designed to avert one embedding process interfering in the other. Watermark embedding in the DFT domain has robust properties respect to rotation, scaling and translation (RST) distortions as well as robustness against common signal processing such as compression, filtering, and noise contamination, among others. The DFT domain embedding algorithm is described as follows:

1) Rescale the color image I into a size of $N_1 \times N_2$, these dimensions will be stored and considered as a secret key K_1 in the detection stage.

2) Since the RGB has the most correlated components while the YCbCr are the less correlated as well as the forward and backward transformations between RGB and YCbCr color models are linear [8], [9], using the information of the image I converts the RGB to YCbCr color model representation and isolates the luminance component $Y(x,y)$ from YCbCr.

3) The watermark is a zero mean 1-D binary pseudo-random pattern formed by {1, 0} values achieved by a secret key K_2, $W = \{w_i|\ i=1, \ldots, L\}$, where L is the length of the watermark.

4) Apply the 2D DFT transform to the original luminance component $Y(x,y)$. The 2D DFT transform of $Y(x,y)$ of size $N_1 \times N_2$ is given by (1):

$$F(u,v) = \sum_{x=1}^{N_1}\sum_{y=1}^{N_2} Y(x,y)\exp\left(-j2\pi(ux/N_1 + vy/N_2)\right). \quad (1)$$

5) Get the magnitude $M(u,v) = |F(u,v)|$ and phase $P(u,v)$ of the $F(u,v)$. By DFT properties [1], the translation in the spatial domain does not affect the magnitude of the DFT transform, as shown in (2):

$$|DFT[Y(x+t_x, y+t_y)]| = M(u,v) \quad (2)$$

where t_x and t_y are the translation parameters in x and y directions, respectively. Meanwhile, the scaling in the spatial domain causes an inverse scaling in the DFT domain, as shown in (3):

$$DFT[Y(s_f x, s_f y)] = \frac{1}{s_f} F\left(\frac{u}{s_f}, \frac{v}{s_f}\right) \quad (3)$$

where s_f is the scaling factor. Concerning the rotation in the spatial domain causes the same rotation in the DFT domain, as shown in (4):

$$DFT[Y(x\cos\theta - y\sin\theta, x\sin\theta + y\cos\theta)] = F(u\cos\theta - v\sin\theta, u\sin\theta + v\cos\theta) \quad (4)$$

where θ is the rotation angle. Then motivation to selecting the DFT domain to embed the watermark W is due to a certain number of advantages for rotation, scaling and translation (RST) invariance as well as robustness against common signal processing. However, the DFT domain presents weak robustness against other aggressive distortions mainly cropping and image corruption by Gaussian noise. Thus, to increase the robustness without decreasing the watermark imperceptibility, in our method, the technique based on CT domain is designed to complement and improve the robustness against the above weakness and is explained later.

6) Select a pair of radiuses r_1 and r_2 in $M(u,v)$ and the annular area $A = \pi(r_2^2 - r_1^2)$ between r_1 and r_2 should cover the middle frequencies coefficients in $M(u,v)$ around the zero frequency term. Because modifications in the lower frequencies of $M(u,v)$ will cause visible distortion in the spatial domain of the image. On the other hand, the coefficients of the higher frequencies are vulnerable to the JPEG compression. Thus, the watermark W should be embedded in the band of the middle frequencies because, in this spectral region, it will be robust against JPEG compression and at the same time imperceptible. The pair of radiuses r_1 and r_2 will be stored and considered as a secret key K_4 in the detection stage.

7) Scramble the watermark data bits to guarantee their security using a secret key K_3.

8) For each watermark data bit w_i a pseudorandom $\{-1,1\}$ g_i pattern with length $A/2$ is assigned according to a predefined secret key K_5. Each g_i value is dependent on w_i in the following way:

$$\begin{cases} +g_i & \text{if} \quad w_i = 0, \\ -g_i & \text{if} \quad w_i = 1. \end{cases} \quad (5)$$

After that, the sum of all random patterns g_i defines the encoded watermark W_e as follows:

$$W_e = \sum_{i=1}^{L} \pm g_i \quad (6)$$

where the sign of each g_i is dependent of w_i value as defined in (5).

9) Considering a linear version of the DS-CDMA, embed the encoded watermark W_e into the magnitude coefficients of the annular area $A/2$ corresponding to the upper half of the original magnitude M that cover the middle frequency, in an additive form:

$$M' = M + \alpha W_e \quad (7)$$

where α is the watermark strength and M, M', are the original and the watermarked magnitude coefficients into the middle-frequency band, respectively. A larger value of α would boost the robustness of the watermark, on the other hand, the watermark imperceptibility is less altered by a small value of α. Hence, there is a tradeoff between robustness and imperceptibility. According to DFT symmetrical properties to produce real values after the DFT magnitude M modification, the watermark was embedded into the upper half part of middle frequencies of the DFT magnitude coefficients, and subsequently, the lower half part of the middle-frequency band should be modified symmetrically.

10) Finally, the watermarked luminance component $Y_w(x,y)$ is obtained applying the inverse DFT (IDFT) to the watermarked magnitude $M'(u,v)$ and the corresponding initial phase $P(u,v)$ as shown follows:

$$Y_w(x,y) = IDFT(F'(u,v)), F' = (M'(u,v), P(u,v)). \quad (8)$$

2.2 Discrete Contourlet Transform Embedding Process

Once the watermarked luminance channel Y_w is acquired, the watermark embedding procedure starts the second method into CT domain and thus getting the watermarked color image, which is explained as follows. Watermark embedding into the chrominance information using the CT domain has robust properties respect to high image cropping, image replacement, rotation with cropping, as well as robustness against common signal processing such as filtering and Gaussian noise contamination, among others. The CT domain embedding process is described as follows:

1) Isolate the blue difference chrominance component $Cb(x,y)$ from YCbCr color model representation. According to the human color vision, color information is detected at normal (daylight) levels of illumination by the three types of photoreceptors denoted as cones, named L, M, S, corresponding to the light sensitive pigments at long, medium, and short wavelengths, respectively [9]. In a global manner and considering that the amount of S-cones is scarce compared with the number of L-M-cones into the human eye, the human color vision is less sensitive to the blue color than it is to the red and green colors.

2) Apply the 2D CT transform to the original blue-difference chrominance component $Cb(x,y)$ with three levels of decomposition.

3) For each watermark data bit w_i a pseudorandom $\{-1,1\}$ pattern h_i is assigned according to a predefined secret key K_6.

4) Using a linear version of the improved spread spectrum watermarking technique [23], [24] embeds the watermark data bits w_i as follows:

$$c_s' = c_s + (\gamma w_i - \lambda z)h_i \tag{9}$$

where c_s and c_s' are the original and watermarked eight CT directional sub-bands of the third decomposition level respectively. Meanwhile, w_i is the i-th watermark data bit, γ is the watermark strength, λ is a distortion control parameter, h_i the i-th pseudorandom sequence and $z \equiv \langle c_s | h_i \rangle / \langle h_i | h_i \rangle$, the operator $\langle A | B \rangle$ denotes inner product and is defined as:

$$\langle A | B \rangle \doteq \frac{1}{N}\sum_{j=1}^{N} A_j B_j \tag{10}$$

where N is the length of some given vectors A and B. From (9), in the conventional spread spectrum watermarking scheme $\lambda = 0$. To simplify the analysis to determinate an optimal value to the distortion control parameter λ, considering only a single watermark data bit w with a given pseudorandom sequence h, as well as the information channel is modeling as additive noise, we get:

$$s = c_s' + n \ , \tag{11}$$

with the channel noise modeled as in (11), the receiver sufficient statistics is:

$$\begin{aligned} r = \frac{\langle s | h \rangle}{\langle h | h \rangle} &= \frac{\langle c_s + (\gamma w - \lambda z)h + n | h \rangle}{\langle h | h \rangle} \\ &= \gamma w + (1-\lambda)z + n \end{aligned} \tag{12}$$

where $n \equiv \langle n | h \rangle / \langle h | h \rangle$. Therefore, from (12) we can see that the closer we make λ to 1, the more the influence of z is removed from r. The optimum value of λ can be computed as in [23] and is given by:

$$\begin{aligned} &\lambda_{\text{optimum}} = 0.5(Q1 - Q2), \\ &Q1 = \left(1 + \frac{\sigma_n^2}{\sigma_{c_s}^2} + \frac{N\sigma_h^2}{\sigma_{c_s}^2}\right), \\ &Q2 = \left(\sqrt{\left(1 + \frac{\sigma_n^2}{\sigma_{c_s}^2} + \frac{N\sigma_h^2}{\sigma_{c_s}^2}\right)^2 - 4\frac{N\sigma_h^2}{\sigma_{c_s}^2}}\right) \end{aligned} \ , \tag{13}$$

where N is the length of n, h and c_s. Variables $\sigma_{c_s}^2$, σ_n^2 and σ_h^2 denote the variances of c_s, n, and h respectively. From (13) we can see that to N large enough, the value of $\lambda_{\text{optimum}} \to 1$ and the signal to noise ratio SNR$\to\infty$. As we can compute the optimum value to λ from (13), we can vary γ to find the best performance of the trade-off imperceptibility- robustness.

5) Then, the watermarked component $Cb_w(x,y)$ is obtained by CT image reconstruction. Thus, the watermarked image I_w is assembled using the watermarked luminance component $Y_w(x,y)$, the watermarked blue difference chrominance component $Cb_w(x,y)$ and the original red difference chrominance component $C_r(x,y)$; restoring the Y_wCb_wCr watermarked components to RGB color model representation. Rescale the watermarked image I_w to the dimensions of the original image I. The diagram of the embedding process is shown in Fig. 1. The secret keys K_1, K_2, K_3, K_4, K_5 and K_6 shown in Fig. 1 are also known by the watermark detector.

2.3 Detection Process

The detection process diagram is shown in Fig. 2, and it is described as follows:

1) Rescale the color watermarked image I_w into a size of $N_1 \times N_2$ using the secret key K_1.

2) Using the information of the image I_w, converts the RGB to YCbCr color model representation and obtain the watermarked components Y_w and Cb_w respectively. If I_w was distorted by a general affine transformation, then, from luminance information Y_w and supported by our resynchronization method previously reported in the literature, we can restore geometrically the attacked image detecting the watermark

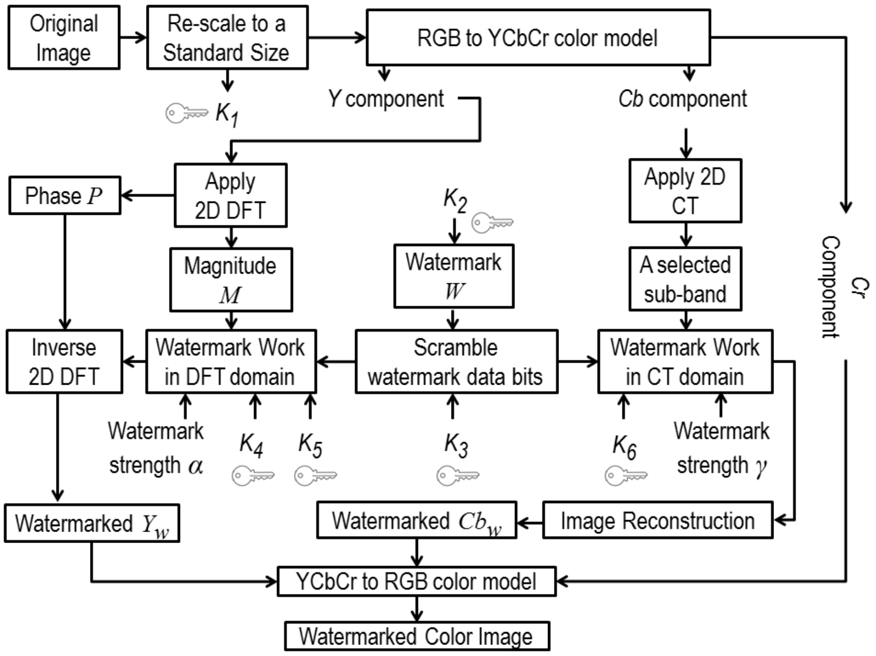

Fig. 1. Flowchart of watermark embedding procedure.

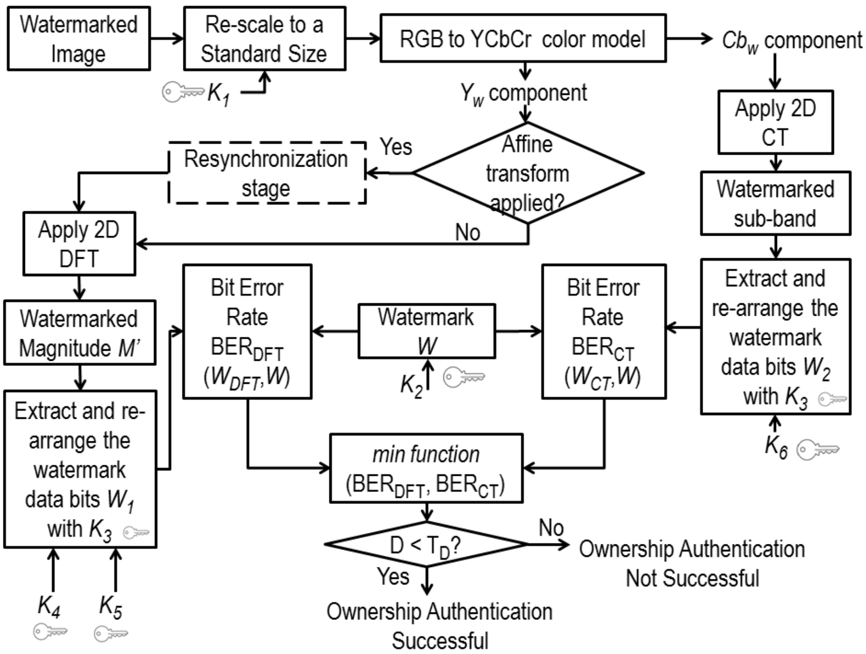

Fig. 2. Flowchart of watermark detection procedure.

correctly. To more details of the resynchronization technique, interested readers can refer to [29].

3) Compute the bi-dimensional DFT transform $F'(u,v)$ of the watermarked luminance component $Y_w(x,y)$. Then from $F'(u,v)$ get the watermarked magnitude $M'(u,v) = |F'(u,v)|$.

4) The annular area A is computed using the secret key K_4 that contains the values of radiuses r_1 and r_2 used in the embedding process.

5) Split the DFT watermarked magnitude $M'(u,v)$ in two parts, the upper half, and the lower half respectively.

6) By symmetrical DFT properties, using only information from the upper half part of watermarked magnitude M', the embedded watermark can be extracted one bit at a time by calculating the correlation between the normalized watermarked magnitude coefficients M'_{norm} and the i-th pseudorandom pattern g_i. Thus, using the secret key K_5, compute the linear correlation C_i^{DFT} between the normalized watermarked magnitude coefficients M'_{norm} and the i-th pseudorandom pattern g_i as follows:

$$C_i^{\text{DFT}} = \sum_{i=1}^{L} ((g_i - \hat{g}_i) \cdot M'_{\text{norm}}) \tag{14}$$

where $\hat{g}_i$ is the average of all values in g_i and $M'_{\mathrm{norm}} = M' - M'_{\mathrm{av}}$, where $M'av$ is the average of all values in M'.

7) Decode the watermark pattern $W_{\mathrm{DFT}}\{w'_i \mid i=1, \ldots, L\}$ using the sign function as follows: if sign(C_i^{DFT}) is '+' then $w'_i = 0$, otherwise $w'_i = 1$. Re-arrange W_{DFT} using the secret key K_3.

8) Using the watermarked blue-difference chrominance component $Cb_{\mathrm{w}}(x,y)$, apply the 2D CT transform with three levels of decomposition.

9) Using only information from the eight sub-bands that compose the third decomposition level, the embedded watermark can be extracted one bit at a time by calculating the linear correlation C_i^{CT} between the watermarked directional sub-band coefficients c_s' of the third CT decomposition level and the pseudo-random sequences h_i as follows:

$$C_i^{\mathrm{CT}} = \sum_{i=1}^{L} (c_s' \cdot h_i) \ . \tag{15}$$

10) Decode the watermark pattern $W_{\mathrm{CT}}\{w'_i \mid i=1, \ldots, L\}$ using the sign function as follows: if sign(C_i^{CT}) is '+' then $w'_i = 0$, otherwise $w'_i = 1$. Re-arrange W_{CT} using the secret key K_3.

11) Reorganize the original watermark pattern W with the secret key K_2 and compute the bit error rate (BER) between (W, W_{DFT}) and (W, W_{CT}) denoted by BER_{DFT} and BER_{CT} respectively.

12) Compare and select the minimum value between BER_{DFT} and BER_{CT} using a min function. The result is indicated as a decision value D.

13) Adopting ergodicity, the BER is defined as the ratio between the number of incorrectly decoded bits and the total number of embedded bits. A decision threshold value T_{D} must be set to determine if the watermark W is present or not into the color image. In this concern, considering a binomial distribution with success probability equal to 0.5, the false alarm probability P_{fa} for L bits embedded watermark data is given by (16), and a threshold value T must be set to ensure that P_{fa} is smaller than a predetermined value.

$$P_{\mathrm{fa}} = \sum_{q=T}^{L} (0.5)^L \cdot \left(\frac{L!}{q!(L-q)!} \right) \tag{16}$$

where L is the total number of watermark data bits, whose value in our experiments is empirically set to 32. The false alarm probability must be less than $P_{\mathrm{fa}} = 5.6537 \times 10^{-5}$, which is to be able to satisfy the requirements of most watermarking applications for a reliable detection. Then an adequate decision threshold value T_{D} ($= 1 - (T/L) = 1 - (27/32)$) is equal to 0.1563, according to the fact that the bit error rate (BER) + the bit correct rate (BCR) must be equal to 1. If $D > T_{\mathrm{D}}$ (more than five error bits) the watermark detection is failed, else if $D < T_{\mathrm{D}}$ the watermark detection is successful and the detection process is terminated.

3. Results and Discussion

In this section, the performance of the proposed algorithm is evaluated considering watermark imperceptibility and robustness properties and using a variety of digital color images. We have used 1000 images with different content among which are Goldhill, Barbara, Lena, Airplane, Baboon, Peppers, among others, all of sizing 512×512 and color resolution of 24bits/pixel. Our experiments were carried out on a personal computer running Microsoft Windows 7© with an Intel© Xeon processor (2.4 GHz) and 16 GB RAM while the embedding and extracting procedures were implemented on Matlab© 8.1. In our system, the average computing time for the embedding process has been 1.64 seconds while an average of 1.13 seconds was needed for the detection procedure. A 1D binary pseudorandom sequence of size $L = 32$ bits is used as the watermark pattern W, which is embedded in a redundant manner as explained, getting a watermark payload of 64. For the Contourlet transform as suggested in [22], we use the 9–7 biorthogonal filters with three levels of pyramidal decomposition for the multi-scale decomposition stage and the 'dmaxflat7' filters for the multidirectional decomposition stage. We partition the finest scale to eight directional sub-bands. The false alarm probability is $P_{\mathrm{fa}} = 5.6537 \times 10^{-5}$ when the decision threshold $T_{\mathrm{D}} = 0.1563$. The values $N_1 = N_2 = 768$ composes the secret key K_1 used. The secret key K_4 is formed by the pair of radiuses employed in the DFT domain embedding process and were $r_1 = 50$ and $r_2 = 150$. The watermark strengths used in the embedding are equal to $\alpha = 1.5$ and $\gamma = 0.3$. The watermarked image quality is measured using the following well-known indices Peak Signal to Noise Ratio (PSNR), Visual Information Fidelity (VIF) [25] and Structural Similarity Index (SSIM) [26]. The difference color of the watermarked image is obtained using the Normalized Color Difference (NCD) measure [27]. Finally, we present a comparison with some previously published methods which reported outstanding results and have a similar purpose as our proposal.

3.1 Setting Parameters r_1, r_2 and Directional Sub-bands c_s

Considering the DFT domain embedding process into the luminance component (Y) from YCbCr color model of the original color image, a watermark strength $\alpha = 1.5$ and $\gamma = 0.3$, a pair of experimental radiuses $r_1 = 5$, $r_2 = 105$ for low, $r_1 = 50$, $r_2 = 150$ for middle and $r_1 = 150$, $r_2 = 250$ for high DFT magnitude frequency respectively, and a value of $L = 32$, in Tab. 1 we show the average VIF after the watermark embedding in each spectral region, obtaining 0.7536 for low, 0.9283 for middle and 0.9633 for high DFT

Visual Information Fidelity		
Low Frequency [r_1 =5, r_2 =105]	**Middle Frequency** [r_1 =50, r_2 =150]	**High Frequency** [r_1 =150, r_2 =250]
VIF=0.7536	VIF=0.9283	VIF=0.9633

Tab. 1. Average VIF after the watermark embedding in each different spectral region.

magnitude frequency respectively. The range of VIF is [0, 1] and the closer value to 1 represents the better fidelity respect to the original image. Then according to the VIF results in Tab. 1, we can see that from the imperceptibility point of view, the modifications in the magnitude of lower frequencies of the DFT will produce visible distortion in the spatial domain of the image.

However, although the magnitude coefficients of the high frequency offer the high watermark imperceptibility, but on the other hand are susceptible to the JPEG compression. Considering the same parameters used in the above experiment, and applying a JPEG lossy compression to the watermarked color image with quality factor equal to 20; in Fig. 3 (a) we show the average BER after the watermark embedding in each spectral region, obtaining 0 for low, 0.0313 for middle and 0.3438 for high DFT magnitude frequency respectively. BER values of the low and middle frequencies are less than the decision threshold value $T_D = 0.1563$. However, BER value of the high frequency is greater than $T_D = 0.1563$, affirming the susceptibility of the high frequency against JPEG compression. Thus, the watermark should be embedded in the range of the middle frequencies $r_1 = 50$, $r_2 = 150$ because, in this spectral region, it will be robust against JPEG compression and at the same time imperceptible. Once that the pair of radiuses $r_1 = 50$ and $r_2 = 150$ are set, we consider the CT domain embedding process, a watermark strength $\alpha = 1.5$, $\gamma = 0.3$ and a value of $L = 32$. Then, use the four, eight and sixteen directional subbands that compose the second, third and fourth CT decomposition levels respectively.

Table 2 shows the average PSNR after the watermark embedding in each decomposition level, obtaining 57.6391 dB for the second, 53.7513 dB for the third and 48.5229 dB for the four decomposition level respectively. According to the PSNR results in Tab. 2, we can see that from the imperceptibility point of view, embedding the watermark into the directional sub-bands of the fourth decomposition level will cause a decreasing of the quality image since PSNR value is less than 49 dB. However, although the embedding into the second decomposition level provides high watermark imperceptibility, it is vulnerable to the image corruption by Gaussian noise. Considering the same parameters used in the above experiment, and applying Gaussian noise contamination to the watermarked color image with mean $\mu = 0$ and variance $\sigma^2 = 0.05$; in Fig. 3(b) we show the average BER after the watermark embedding in each decomposition level, obtaining 0.1875 for the second, 0.0313 for the third and 0 for the four decomposition level, respectively. BER values of the third and fourth decomposition level are less than the decision threshold value $T_D = 0.1563$. But, BER value of the second decomposition level is greater than $T_D = 0.1563$, confirming the vulnerability of the embedding into the second decomposition level against Gaussian noise. Thus, in our proposed method, the watermark should be embedded in the directional sub-bands of the third decomposition level because, in this spectral region, it will be robust against Gaussian noise and at the same time imperceptible.

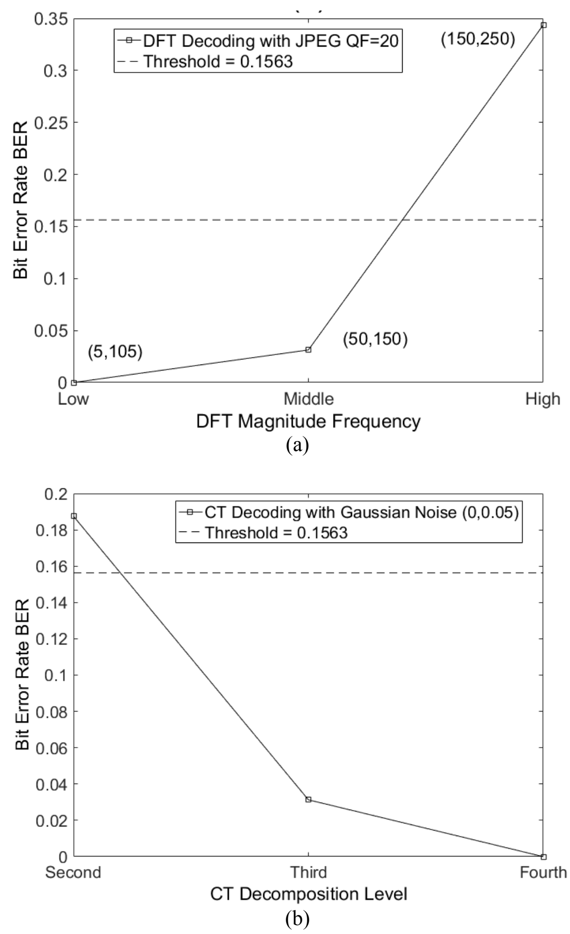

Fig. 3. (a) Average BER after DFT decoding in each spectral region: BER = 0 for low, BER = 0.0313 for middle and BER = 0.3438 for high DFT magnitude frequency respectively. (b) Average BER after CT decoding in each decomposition level: BER = 0 for the 4th, BER = 0.0313 for the 3rd and BER = 0.1875 for the 2nd, respectively.

Peak Signal to Noise Ratio PSNR		
2nd Decomposition Level [4 directional sub-bands]	**3rd Decomposition Level** [8 directional sub-bands]	**4th Decomposition Level** [16 directional sub-bands]
57.6391 dB	53.7513 dB	48.5229 dB

Tab. 2. Average PSNR after the watermark embedding in each CT decomposition level.

3.2 Watermark Imperceptibility: Setting Watermark Strength α and γ

As explained in Sec. 3.1 the proposed algorithm embeds a watermark sequence twice using two different frequency domains, i.e., DFT and CT respectively. In this

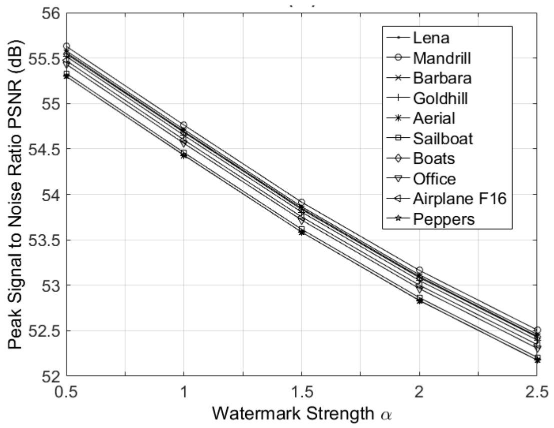

(a)

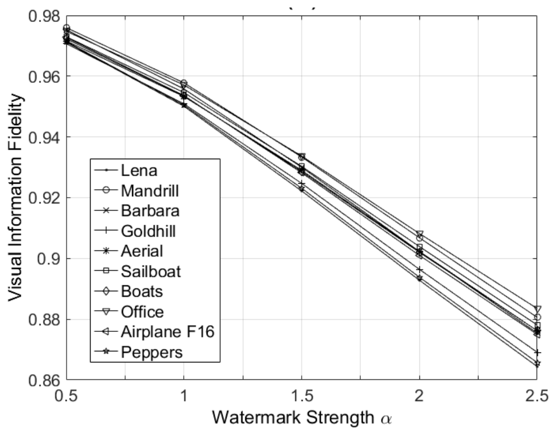

(b)

Fig. 4. Average (a) PSNR and (b) VIF with variable *α*.

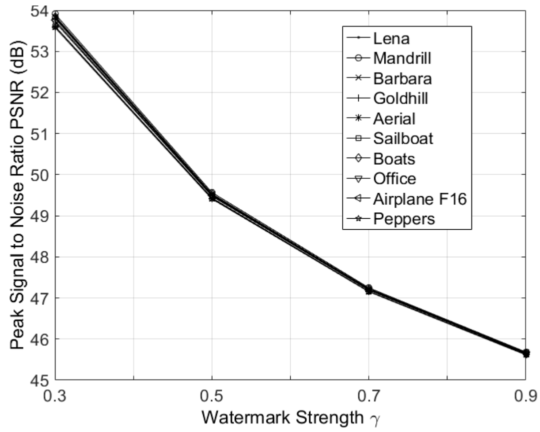

(a)

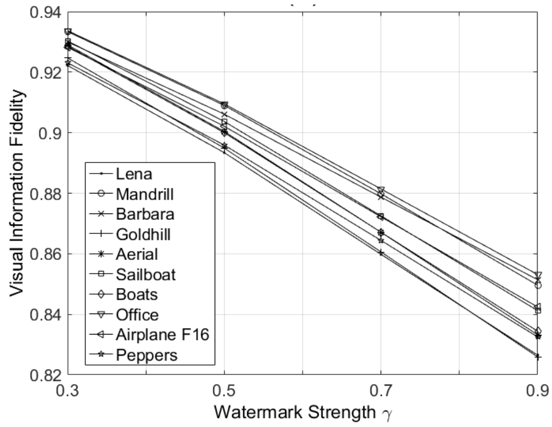

(b)

Fig. 5. Average (a) PSNR and (b) VIF with variable *γ*.

way, a careful watermark imperceptibility evaluation is required. To set the watermark strength α, using a pair of radiuses $r_1 = 50$ and $r_2 = 150$ in DFT domain, watermark length $L = 32$, variable α from 0.5 to 2.5, and a set of ten test color images. The watermark imperceptibility is evaluated regarding the PSNR and VIF image quality metrics. As it is known in the literature, the VIF value reflects perceptual distortions more precisely than PSNR. In Fig. 4, the average PSNR and VIF are plotted with variable watermark strength α ranging from 0.5 to 2.5 respectively.

As shown in Fig. 4(a) and (b), a larger value of α would boost the robustness of the watermark, but the watermark imperceptibility is decreased. Hence, there is a trade-off between robustness and imperceptibility. To preserve the trade-off between robustness and imperceptibility, based on the experimentation, we considered a watermark strength of $\alpha = 1.5$ as a suitable value. To set the watermark strength γ, using the eight directional sub-bands of the third CT decomposition level, watermark length $L = 32$, variable watermark strength γ from 0.3 to 0.9, and a set of ten test color images; the watermark imperceptibility was evaluated regarding the PSNR and VIF image quality metrics. In Fig. 5, the average PSNR and VIF are plotted with variable watermark strength γ ranging from 0.3 to 0.9 respectively. As shown in Fig. 5(a) and (b), a larger value of γ would boost the robustness of the watermark, but the watermark imperceptibility is declined.

Image	PSNR (dB)	VIF	SSIM	NCD
Lena	53.8638	0.9222	0.9872	0.0240
Baboon	53.9135	0.9334	0.9947	0.0248
Barbara	53.8461	0.9300	0.9882	0.0318
Goldhill	53.8047	0.9247	0.9886	0.0364
Sailboat	53.6154	0.9303	0.9899	0.0274
Boats	53.8335	0.9286	0.9865	0.0305
Office	53.7169	0.9337	0.9891	0.0270
Airplane	53.7516	0.9282	0.986	0.0202
Peppers	53.5839	0.9231	0.9875	0.0213
Aerial	53.5838	0.929	0.9931	0.0320

Tab. 3. Watermark imperceptibility measured regarding PSNR, VIF, SSIM and NCD metrics.

Hence, once again there is a trade-off between robustness and imperceptibility. To preserve the trade-off between robustness and imperceptibility, based on our experiments, we considered a watermark strength of $\gamma = 0.3$ as a suitable value.

According to the results of Figs. 4 and 5, establishing the watermark strength $\alpha = 1.5$ and $\gamma = 0.3$ we obtain a PSNR greater than 53 dB and the VIF value near to 1, it follows that the proposed technique preserves the trade-off between robustness and imperceptibility.

In order to complement the watermark imperceptibility evaluation, using $r_1 = 50$ and $r_2 = 150$, $\alpha = 1.5$, $\gamma = 0.3$, the eight directional sub-bands of the third CT decomposition level and a watermark with $L = 32$, in Tab. 3 we show the values of PSNR, VIF, SSIM and NCD of watermarked test images respect to the original ones, and in Fig. 6, some original images (a-c) together with their respective watermarked versions (d-f) are shown.

From Tab. 3 and Fig. 6, it follows that the proposed watermarking algorithm provides a sufficiently good fidelity of the watermarked color image, and also the color difference provided by NCD metric, between the watermarked image and the original one is insignificant [27], i.e., is near to 0.

From Tab. 3 we show that the average PSNR is greater than 53 dB, and the SSIM, as well as VIF values obtained, are near to 1. The range of SSIM is [0, 1], and the closer value to 1 represents the better quality respect to the original image, a value SSIM = 1 indicates that the original and the reference image are the same. In this manner, it follows that the proposed scheme provides a fairly good fidelity of the watermarked image.

The imperceptibility performance is compared with results reported by algorithms [20] and [21] respectively, which to the best of our knowledge are the most robust watermarking algorithms published applied to color images, with similar purposes as our proposed scheme. To

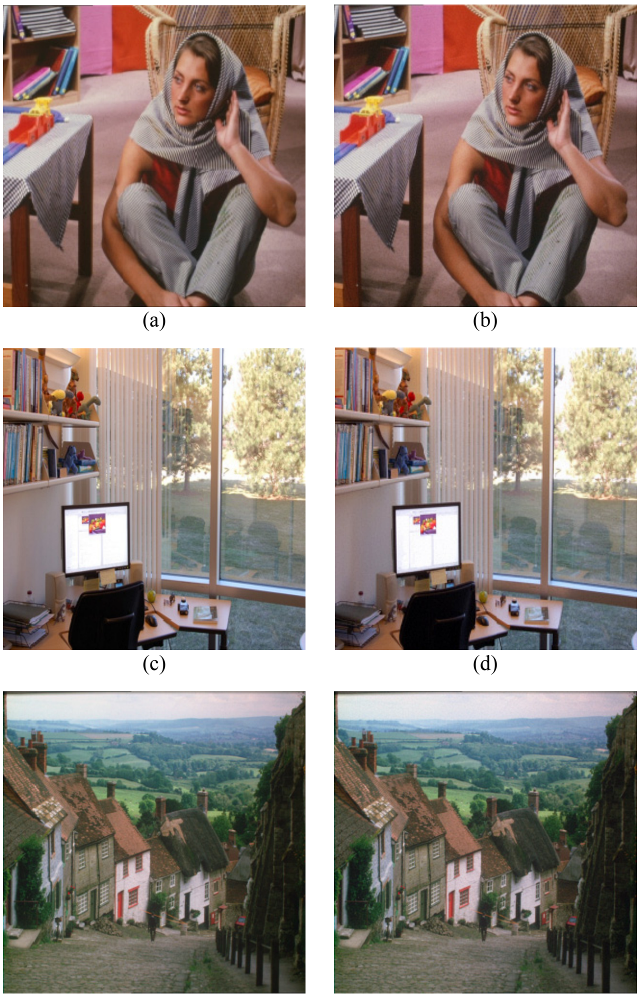

(a) (b) (c) (d) (e) (f)

Fig. 6. Original (a), (c), (e), Watermarked versions (b), (d), (f).

Image	Proposed Method	Pan-Pan et al. [20]
Lena	53.87 dB	40.57 dB
Baboon	53.91 dB	41.67 dB
Barbara	53.85 dB	40.71 dB

Tab. 4. Comparison of watermark imperceptibility in terms of PSNR between our method and Pan-Pan et al. [20].

Image	Proposed Method	Prathap et al. [21]
Lena	53.87 dB	54.68 dB
Baboon	53.91 dB	53.55 dB
Peppers	53.58 dB	58.32 dB

Tab. 5. Comparison of watermark imperceptibility in terms of PSNR between our method and Prathap et al. [21].

get a proper comparison, we consider a homogeneous format of color images of $512 \times 512 \times 24$ bits. The comparison results are shown in Tab. 4 and 5.

From Tab. 4 and 5 it follows that our proposed method provides a reasonably good fidelity of the watermarked color image, achieving a PSNR greater than 53 dB, avoiding the perceptual distortions in the color images.

Comparison results show that the PSNR results of the method reported by Pan-Pan et al. in [20] are clearly outperformed by our proposed method. Meanwhile, the imperceptibility results obtained by Prathap et al. in [21] and our proposed method are very similar, achieving PSNR greater than 53 dB.

3.3 Watermark Robustness

To evaluate the watermark robustness of the proposed algorithm, several geometrical, signal processing, and combined distortions are applied to watermarked color images. In the flowchart showed in Fig. 2 and described in detail in Sec. 2.3, the watermark detector makes a decision based on two calculated BER values that correspond in turn to each watermark embedding process introduced in this proposal.

To have a clear perception of robustness achieved by each watermark decoding against performed distortions, the output of each detector is displayed separately in a form CT/DFT linked to the Contourlet Transform/Discrete Fourier Transform decoding respectively. In this way, the strengths and weakness of each embedding method can be precisely determined. Tab. 6, 7 and 8 show the BER obtained after applying the distortions mentioned above to a set of six test watermarked images. In Tab. 6, 7 and 8 italic characters indicate failure detection against the respective distortion.

From Tab. 6 and considering the decision value *D* criterion described in Sec. 2.3, we can observe that the embedded watermark signal in our proposed method is sufficiently robust to most common signal processing distortions. These distortions including JPEG lossy compression with quality factor until 10, Gaussian and median filtering with different size windowing, sharpening, brightness, and image corruption by the determined amount of Gaussian and impulsive noise respectively, histogram equalization, motion blurring, gamma correction and visual watermark added into RGB channels. Obtaining BER values less than the decision threshold $T_D = 0.1563$, calculated as mentioned in Sec. 2.3, and used to determine if the watermark W is present or not in the watermarked color image.

From Tab. 7 we can observe that our proposed method is sufficiently robust to geometric attacks. These distortions including all rotation angles with and without cropping, image scaling with several scale factors, dynamic image cropping until 95%, centered cropping, image replacement, translation with removal columns and rows, general affine transformations including shearing in x-direction and aspect ratio changes. In all cases, using the decision value D criterion, we obtained BER values less than the decision threshold $T_D = 0.1563$.

To complement the robustness testing, we design a set of combined distortions composed by JPEG lossy compression with quality factor 50 in conjunction with several common signal processing and geometric distortions shown in Tab. 6 and 7 respectively. According to the experimental results, from Tab. 8 we demonstrate that the proposed method is robust against this kind of combined distortions, obtaining BER values less than $T_D = 0.1563$.

With illustrative purposes, in Fig. 7 we show the Airplane watermarked image after being processed by six of the most aggressive distortions. In all cases, the BER value is less than the decision threshold $T_D = 0.1563$.

The robustness performance is compared with that reported by the algorithms [20] and [21] respectively. Again, to get a proper comparison, we consider a homogeneous format of color images of $512 \times 512 \times 24$ bits. To design a compact robustness testing, the set of distortions discussed in the comparative include only the most aggressive distortions reported in the literature. Tab. 9 and 10 show the robustness relative in BER terms with that reported by the algorithms [20] and [21] respectively.

From Tab. 9 we show that the algorithm of Pan-Pan et al. [20] and our proposed watermarking method are robust against several geometric distortions including rotation, scaling, translation, cropping, affine transformation and aspect ratio changes. Both proposals are robust against signal processing including JPEG compression, median, and Gaussian filtering, sharpening, impulsive and Gaussian noise. Moreover, both methods are robust to the combined distortions composed by operations of the same type, i.e., geometric/geometric or signal processing/signal processing respectively. However, the method of Pan-Pan et al. [20] is outperformed by our proposed method because in almost all test our method get BER values close to 0. Moreover, the tolerance of Pan-Pan et al. [20] against several distortions is weak compared with the tolerance of our proposed method, which was previously shown in Tab. 6, 7 and 8. Furthermore, our proposal considers a broader range of distortions compared with the reported by Pan-Pan [20].

From Tab. 10 we show that the algorithm of Prathap et al. [21] and our proposed watermarking method are robust against several geometric distortions including a rotation with and without cropping, scaling, translation, and cropping. Meanwhile, both approaches are robust against signal processing including JPEG compression, median, and Gaussian filtering, sharpening, impulsive and Gaussian noise. Moreover, both approaches are robust to the combined distortions composed JPEG lossy compression with quality factor 50 in conjunction with signal processing or geometric distortion. However, the method of Prathap et al. [21] is outperformed by our proposed method

Distortion	Lena CT/DFT	Baboon CT/DFT	Barbara CT/DFT	Goldhill CT/DFT	Peppers CT/DFT	Airplane CT/DFT
Without attack	0/0	0/0	0/0	0/0	0/0	0/0
JPEG 90	0/0	0/0	0/0	0/0	0/0	0/0
JPEG 70	*0.1875*/0	0.125/0	*0.2813*/0	*0.2188*/0	*0.4063*/0	*0.2188*/0
JPEG 50	*0.2813*/0	*0.2188*/0	*0.4063*/0	*0.2188*/0	*0.4375*/0	*0.375*/0
JPEG 20	*0.4063*/0.0313	*0.25*/0	*0.5938*/0	*0.4063*/0	*0.5313*/0.0313	*0.4063*/0.0625
JPEG 10	*0.5*/0.0313	*0.3125*/0	*0.6563*/0.0625	*0.3438*/0.125	*0.4063*/0.0625	*0.5313*/0.125
Gaussian filter 5x5	0/0	0/0	0/0	0/0	0/0	0/0
Gaussian filter 7x7	0/0	0/0	0/0	0/0	0/0	0/0
Sharpen	0/0	0/0	0/0	0/0	0/0	0/0
Median filter 3x3	0/0	0/0	0/0	0/0	0/0	0/0
Median filter 5x5	0/*0.1875*	0.0938/*0.25*	0/0.0938	0/0.1563	0.0313/*0.1875*	0.0625/*0.2813*
Brightness	0/0	0/0	0/0	0/0	0/0	0/0.0313
Gaussian noise (0,0.06)	0.0313/0.1563	0.0313/0.125	0.0313/0.125	0.0313/0.0625	0.0313/0.0938	0.0313/0.0313
Gaussian noise (0,0.07)	0.0313/*0.2188*	0.0313/0.1563	0.0313/*0.1875*	0.0625/0.1563	0.0625/*0.25*	0.0313/0.0938
Impulsive noise density 0.08	0/0	0/0	0/0	0/0.0938	0/0.0313	0/0.0313
Impulsive noise density 0.09	0/0.0313	0/0	0/0	0/0.0625	0/0.0625	0/0
Histogram equalization	0/0	0/0	0/0	0/0	0/0	0/0
Motion blurring	0/0	0/0.0313	0/0	0/0	0/0	0/0
Gamma correction	0/0	0/0	0/0	0/0	0/0	0/0
Visual watermark added	0/0	0/0	0/0	0/0	0/0	0/0

Tab. 6. BER of CT/DFT decoding respectively obtained from six test watermarked images after signal processing distortions. Decision threshold value $T_D = 0.1563$.

Distortion	**Lena CT/DFT**	**Baboon CT/DFT**	**Barbara CT/DFT**	**Goldhill CT/DFT**	**Peppers CT/DFT**	**Airplane CT/DFT**
Rotation 35° with crop	0/0	0/0	0/0	0/0	0/0	0/0
Rotation 75° with crop	0/0	0/0	0/0	0/0	0/0	0/0
Rotation 195° with crop	0/0	0/0	0/0	0/0	0/0	0/0
Scaling 0.3	0/*0.25*	0.0313/*0.25*	0/*0.1875*	0/*0.1875*	0.0313/0.125	0/*0.3125*
Scaling 0.5	0/0	0/0	0/0	0/0	0/0	0/0
Scaling 0.7	0/0	0/0	0/0	0/0	0/0	0/0
Scaling 1.5	0/0	0/0	0/0	0/0	0/0	0/0
Scaling 2.0	0/0	0/0	0/0	0/0	0/0	0/0
Cropping 65%	0/0	0/0.1563	0/0	0/0.0313	0/0.0625	0/0.0938
Cropping 95%	0/*0.4563*	0/*0.4875*	0/*0.4938*	0/*0.5000*	0/*0.5000*	0/*0.5000*
Centered cropping 100x100	0/0	0/0	0/0	0/0	0/0	0/0
Image replacement	0/0.0625	0/0.0313	0/0.0625	0/0.125	0/0.125	0/0.125
Rotation 45° without crop	0/0	0/0	0/0	0/0	0/0	0/0
Rotation 105° without crop	0/0	0/0	0/0	0/0	0/0	0/0
Rotation 285° without crop	0/0	0/0	0/0	0/0	0/0	0/0
Translation x=30, y=30	*0.6563*/0	*0.6563*/0	*0.5313*/0	*0.625*/0	*0.4063*/0	*0.4063*/0
Translation x=70, y=70	*0.4375*/0.0313	*0.5625*/0.0313	*0.4375*/0	*0.5*/0	*0.5*/0	*0.5625*/0.0313
Aspect ratio (1.2:1)	0/0	0/0	0/0	0/0	0/0	0/0
Aspect ratio (0.7:1.2)	0/0	0/0	0/0	0/0	0/0	0/0
Shearing 0.2x	*0.2813*/0	*0.2813*/0	*0.2500*/0	*0.4688*/0	*0.5313*/0	*0.3125*/0
Affine [0.9,0.2,0;0.1,1.2,0;0,0,1]	*0.375*/0	*0.3125*/0	*0.2813*/0	*0.4375*/0	*0.4688*/0	*0.3438*/0
Affine [1.01,0.1,0;0.1,0.9,0;0,0,1]	*0.4375*/0	*0.4688*/0	*0.25*/0	*0.25*/0	*0.3438*/0	*0.4375*/0

Tab. 7. BER of CT/DFT decoding respectively obtained from six test watermarked images after geometric distortions. Decision threshold value $T_D = 0.1563$.

Combined distortions composed by JPEG compression 50 + *distortion*	**Lena CT/DFT**	**Baboon CT/DFT**	**Barbara CT/DFT**	**Goldhill CT/DFT**	**Peppers CT/DFT**	**Airplane CT/DFT**
Gaussian filter 7x7	*0.25*/0	*0.25*/0	*0.375*/0	*0.3125*/0	*0.4063*/0	*0.3438*/0
Sharpen	*0.3125*/0	*0.3438*/0	*0.375*/0	*0.25*/0	*0.3438*/0	*0.3438*/0
Brightness	*0.375*/0	*0.2188*/0	*0.25*/0	*0.25*/0	*0.5*/0.0313	*0.3438*/0
Gaussian noise (0,0.02)	*0.5*/0	*0.4688*/0.0313	*0.5*/0.0313	*0.4688*/0	*0.5*/0.0938	*0.5*/0.0313
Impulsive noise density 0.05	*0.4688*/0.0313	*0.4375*/0	*0.5*/0.0313	*0.5*/0.0938	*0.5625*/0.0313	*0.5*/0.0313
Median filter 3x3	*0.3438*/0	*0.25*/0	*0.3125*/0	*0.2813*/0	*0.375*/0	*0.375*/0
Histogram equalization	*0.375*/0	*0.2813*/0	*0.4375*/0	*0.2188*/0	*0.375*/0	*0.4063*/0
Gamma correction	*0.2813*/0	*0.1875*/0	*0.25*/0	*0.2188*/0	*0.4375*/0	*0.3125*/0
Visual watermark added	*0.3125*/0.0313	*0.2188*/0	*0.3438*/0	*0.2813*/0	*0.3125*/0	*0.4375*/0.0313
Rotation 35° with crop	*0.4375*/0	*0.4688*/0.0313	*0.4375*/0	*0.4375*/0	*0.4375*/0	*0.4688*/0.0313
Rotation 145° with crop	*0.375*/0.0313	*0.4375*/0	*0.4063*/0	*0.4063*/0	*0.4063*/0	*0.4063*/0.0625
Scaling 0.5	*0.2813*/0	*0.2188*/0	*0.4063*/0	*0.25*/0	*0.375*/0	*0.375*/0
Scaling 2.0	*0.3438*/0	*0.2188*/0	*0.375*/0	*0.2813*/0	*0.3438*/0	*0.3438*/0
Cropping 40%	*0.3125*/0	*0.2188*/0	*0.3125*/0	*0.1875*/0	*0.3438*/0.0313	*0.25*/0
Centered cropping 100x100	*0.375*/0.0313	*0.2813*/0	*0.4063*/0	*0.3125*/0	*0.4688*/0.0313	*0.3438*/0
Rotation 15° without crop	*0.3438*/0	*0.2813*/0	*0.4688*/0	*0.2188*/0	*0.4063*/0	*0.375*/0
Rotation 125° without crop	*0.375*/0	*0.2813*/0	*0.4688*/0	*0.1875*/0	*0.4063*/0	*0.4375*/0
Translation x=30, y=30	*0.4375*/0	*0.4688*/0.0313	*0.5*/0	*0.625*/0	*0.375*/0.0313	*0.5*/0.0313
Aspect ratio (1.2:1)	*0.3438*/0	*0.25*/0	*0.5313*/0	*0.2188*/0	*0.375*/0	*0.375*/0
Aspect ratio (0.7:1.2)	*0.375*/0	*0.3125*/0	*0.4688*/0	*0.2813*/0	*0.3438*/0	*0.375*/0
Shearing 0.2x	*0.6875*/0	*0.4688*/0	*0.625*/0.0625	*0.4688*/0	*0.375*/0	*0.4375*/0.0313
Affine [0.9,0.2,0;0.1,1.2,0;0,0,1]	*0.5625*/0	*0.375*/0	*0.4688*/0.0313	*0.5*/0	*0.5313*/0	*0.375*/0

Tab. 8. BER of CT/DFT decoding respectively obtained from six test watermarked images after combined distortions. Decision threshold value $T_D = 0.1563$.

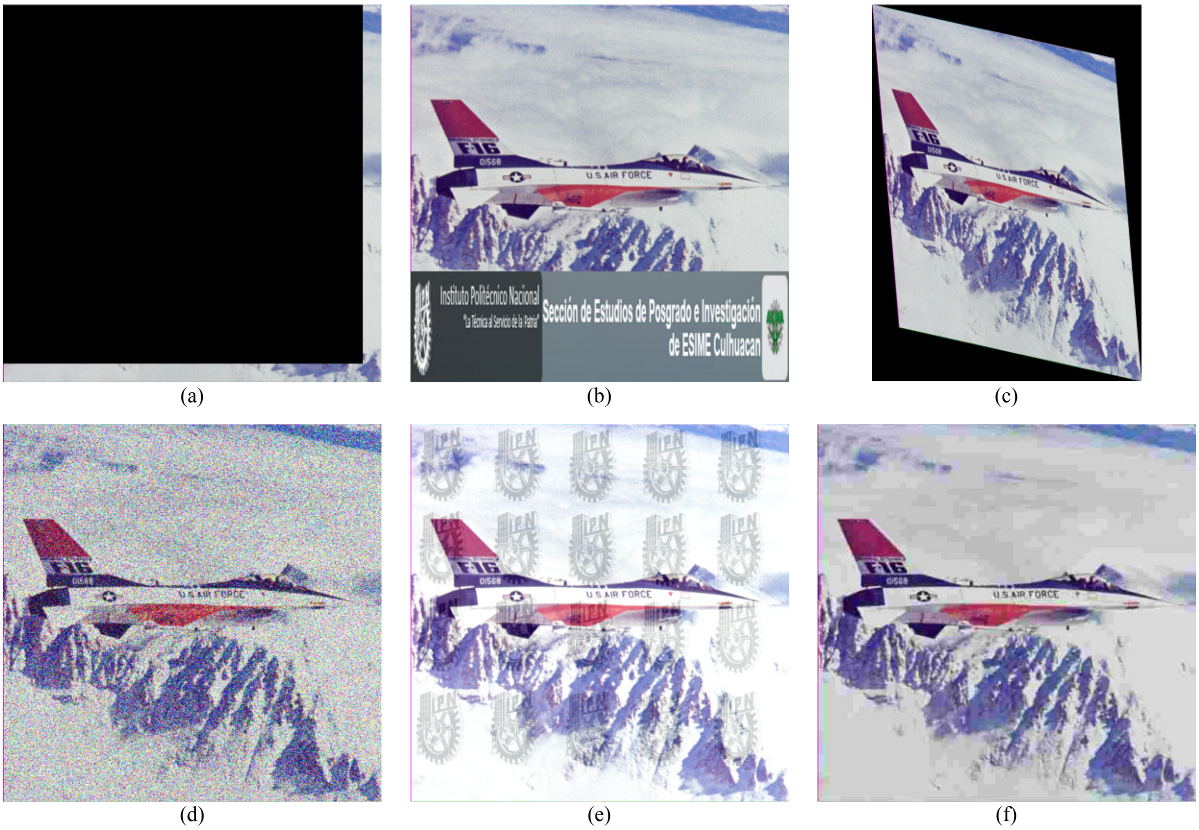

Fig. 7. Aggressive geometric and signal processing distortions in Airplane watermarked image. (a) Cropping with 95%, BER = 0. (b) Image replacement, BER = 0. (c) Affine transformation, BER = 0. (d) Gaussian noise (0,0.07), BER = 0.0313. (e) Visual watermark added, BER = 0. (f) JPEG with QF = 10, BER = 0.125.

Distortion	Lena		Baboon		Barbara	
	Proposed	Ref.[20]	Proposed	Ref.[20]	Proposed	Ref.[20]
JPEG 50	0	0.0334	0	0.0293	0	0.0244
JPEG 30	0	0.0400	0	0.0322	0	0.0283
Median filter 3x3	0	0.0303	0	0.0049	0	0.0234
Gaussian filter 3x3	0	0.0313	0	0.0107	0	0.0225
Sharpen	0	0.0225	0	0.0449	0	0.0273
Gaussian noise (0,0.006)	0	0.0273	0	0.0234	0	0.0215
Impulsive noise density 0.003	0	0.0234	0	0.0205	0	0.0164
Median filter 3x3 + Gaussian Noise (0,0.006)	0	0.0244	0	0.0137	0	0.0186
Gaussian Noise (0,0.006) + Sharpen	0	0.0449	0	0.0811	0	0.0547
JPEG 70 + Gaussian filter 3x3	0	0.0381	0	0.0234	0	0.0303
JPEG 70 + Median filter 3x3	0	0.0264	0.0313	0.0195	0	0.0196
Rotation 45° without crop	0	0.0342	0	0.0164	0	0.0244
Scaling 2	0	0.0273	0	0.0137	0	0.0303
Translation x=20,y=20	0	0.1240	0	0.0605	0	0.1201
Cropping 50%	0	0.1250	0	0.1240	0	0.1250
Aspect ratio (1.2,1.0)	0	0.0244	0	0.0166	0	0.0244
Affine transformation [10; 1.0, 1.0; 0.5, 0.2]	0	0.0225	0	0.0137	0.0313	0.0195
Scaling 2 + Translation x=5,y=0	0	0.0596	0	0.0273	0	0.0713
Rotation 5° + Scaling 2	0	0.0332	0	0.0234	0	0.0254
Rotation 5° + Translation x=5, y=15	0	0.0498	0	0.0479	0	0.1240
Rotation 45° + Scaling 2 + Translation x=20, y=20	0	0.0709	0	0.1318	0	0.1221

Tab. 9. Comparison of BER of extracted watermark for our proposed method and Pan-Pan et al. [20].

Distortion	Lena		Baboon		Peppers	
	Proposed	**Ref.[21]**	**Proposed**	**Ref.[21]**	**Proposed**	**Ref.[21]**
JPEG 50	0	0.0256	0	0.0359	0	0.0417
JPEG 20	0.0313	0.0369	0	0.0381	0.0313	0.0396
JPEG 10	0.0313	0.0359	0	0.0379	0.0625	0.0336
Median filter 5x5	0	0.0435	0.0938	0.0401	0.0313	0.0372
Gaussian filter 7x7	0	0	0	0	0	0
Sharpen	0	0.0241	0	0.0412	0	0.0464
Gaussian noise (0,0.05)	0	0.0485	0	0.0407	0	0.0487
Impulsive noise density 0.08	0	0.0393	0	0.0320	0.0313	0.0355
Rotation 10° without crop	0	0.0370	0	0.0610	0	0.0410
Rotation 45° without crop	0	0.0660	0	0.0510	0	0.0770
Scaling 0.3	0	0.0463	0.0313	0.0534	0.0313	0.0478
Scaling 0.5	0	0.0523	0	0.0623	0	0.0701
Rotation 10° with crop	0	0.0290	0	0.0590	0	0.0280
Rotation 60° with crop	0	0.0510	0	0.0690	0	0.0460
Translation x=40,y=40	0	0.05	0	0.0560	0	0.0380
Cropping 25%	0	0.0410	0	0.0435	0	0.0523
JPEG 50 + Median Filter 3x3	0	0.0429	0	0.0443	0	0.0471
JPEG 50 + Gaussian Noise (0,0.01)	0	0.0448	0	0.0261	0	0.0322
JPEG 50 + Scaling 0.2	0.0625	0.0625	0.0938	0.0436	0.0939	0.0666

Tab. 10. Comparison of BER of extracted watermark for our method and Prathap et al. [21].

Comparison	Najih, et al. [6]	Xiang-Yang, et al. [7]	Chrysochos et al. [16]	Shao-Li. [18]	Pan-Pan et al. [20]	Prathap et al. [21]	Proposed Method
JPEG (Quality Factor)	Detected	20 – 80	25 – 100	10 – 100	30 – 100	5 – 100	10 – 100
Scaling	0.5 – 1	0.5 – 1.5	Detected	0.5 – 2.5	0.5 – 2	0.2 – 1	0.3 – 2
Cropping	Up to 25%	Up to 25%	Up to 20%	Up to 50%	Up to 20%	Up to 25%	Up to 95%
Affine Transformation	-	-	-	-	Detected	-	Detected
Rotation	Detected	0° – 45°	0° – 360°	0° – 30°	0° – 45°	0° – 90°	0° – 360°
Visual Watermark Added	-	-	-	-	-	-	Detected
Image Replacement	-	-	-	-	-	-	Detected
Gaussian Noise	(0, 0.01)	(0, 0.01)	(0, 0.95)	(0, 0.25)	(0, 0.006)	(0, 0.01)	(0, 0.07)
Combined Distortions - Geometric (G) - Signal Processing (SP)	-	a) JPEG50 + (G) or (SP)	-	-	a) JPEG70 + (SP) b) (G) + (G) c) (SP) + (SP)	a) JPEG50 + (SP) or (G) (b) (G) + (G)	a) JPEG50 + (G) or (SP) b) (G) + (G) c) (SP) + (SP)
Watermark Length (bits)	Not Provided	Not provided	30	1024	1024	200	64
Image Quality Metrics	Average PSNR 61dB	Not measured	Average: wPSNR=50dB PSNR=37dB	Average SSIM 0.9887	Average PSNR 40.98dB	Average PSNR 53.55dB	Average: PSNR=53.75dB SSIM=0.989 VIF=0.928 NCD=0.02
Image kind	Grayscale	Grayscale	Grayscale	Color	Color	Color	Color

Tab. 11. Performance comparison.

because in almost all test our method get BER values close to 0. Moreover, the method of Prathap et al. [21] is not robust to affine transformations and its tolerance against image cropping attacks is weak compared with the tolerance of our proposed method, which was previously shown in Tab. 6, 7 and 8. Furthermore, our proposal considers a broader range of distortions compared with [21].

3.4 Robustness against Geometric Distortions

According to the experimental results, our proposed watermarking method presents a high robustness against a broader range of distortions. Focusing on the geometric distortions, the robustness against rotations with and without cropping is obtained through exhaustive search from 0° to 180° rotation degrees to DFT decoding (by symmetrical properties) and 0° to 360° to CT decoding. On the other hand, the use of the secret key K_1 that re-scales the color image to a standard size allows robustness against scaling and aspect ratio changes. Moreover, the method is robust against aggressive cropping, which is considered as a correlated noise, because the DS-CDMA and ISS spread spectrum techniques preserve the second Shannon's theorem [30]. Finally, our method presents robustness against general affine transformations because when a watermarked color image is deformed with an affine operation, from luminance information and supported by our resynchronization method previously reported in the literature, we can restore geometrically the attacked image detecting the watermark correctly. To more details of the resynchronization technique, interested readers can refer to [29].

3.5 Payload

Since our design implies an ownership authentication application, to preserve the trade-off between imperceptibility and robustness we consider a watermark length $L = 32$ as optimal value to determine the presence or absence of watermark with a false alarm probability $P_{fa} = 5.6537 \times 10^{-5}$, which is to be able to satisfy the requirements of ownership authentication applications. Because our method embeds the watermark by duplicate, the total payload of our proposed method is 64 watermark data bits.

3.6 Security

In addition to robustness and imperceptibility, the security of our scheme is another important aspect to consider. Then, the security level is defined by the number of observations the opponent needs to estimate the secret keys [28], [31] accurately. It is ensured by the set of six secret keys K_1, K_2, K_3, K_4, K_5 and K_6, which additionally could be renewed periodically by the ownership to keep the security level and avoid the watermark removal.

3.7 Performance Comparison

Finally, this investigation compares the performance of the proposed method with the algorithm based on angle quantization in discrete Contourlet transform developed by Najih, et al. [6] in 2016, the algorithm based on the exponent moments invariants in non-subsampled Contourlet transform domain proposed by Xiang-Yang, et al. [7] in 2014, the hybrid watermarking based on chaos and histogram modification proposed by Chrysochos et al. [16] in 2014, the watermarking to color images based on Singular Value Decomposition (SVD) developed by Shao-Li. [18] in 2014, the color image watermarking scheme in non-sampled Contourlet-domain proposed by Pan-Pan et al. [20] in 2011, and the hybrid robust watermarking for color images proposed by Prathap et al. [21] in 2014, under JPEG lossy compression, scaling, cropping, affine transformation, rotation, visual watermark added, image replacement, Gaussian noise and combined distortions. Table 11 compares the performance of the watermark detector outputs, the watermark data length, image quality metrics and the kind of image associated with each algorithm. Table 11 presents also the tolerance under distortions, and designates the capacity to resist as ‘detected’, when the tolerance is not given in detail by the other six methods above mentioned. A grid-cell is marked with a dash for attack simulations not mentioned in the literature. These results show better performance of the proposed method compared with principal methods reported previously in terms of imperceptibility and robustness against most common geometric, signal processing and combined attacks.

4. Conclusions

In this paper, we have designed a high robust, blind, color image watermarking algorithm which employs DS-CDMA and ISS watermark embedding in both DFT and CT domain respectively. This method is applicable for ownership authentication of color pictures. The proposed scheme can tolerate a broader range of distortions, particularly signal processing, geometric and combined distortions. Authenticity is achieved by the thresholding criterion regarding bit error rate. Our proposed method satisfies the primary watermarking requirements such as imperceptibility, security, and robustness. Algorithm is very robust against geometric manipulations including rotation by several angles with and without cropping, affine transformation, image replacement, scaling, aspect ratio change, aggressive cropping attacks among others. Also, the method is robust against several common signal processing distortions such as JPEG lossy compression, median and Gaussian filtering, impulsive and Gaussian noise perturbation, brightness, contrast, visual watermark added, sharpening, and histogram equalization among others. The method presents good robustness against combined distortions composed by several geometric and signal processing attacks. The comparison of the proposed method with other existing schemes shows the improved performance in terms of imperceptibility and robustness, in the context of robust watermarking techniques.

Acknowledgments

Authors thank the Instituto Politecnico Nacional (IPN), the Consejo Nacional de Ciencia y Tecnologia de Mexico (CONACyT) as well as the Post-Doctorate Scholarships program and the PAPIIT IN106816 project from DGAPA in Universidad Nacional Autonoma de Mexico (UNAM) by the support provided during the realization of this research.

References

[1] BARNI, M., BARTOLINI, F. *Watermarking Systems Engineering: Enabling Digital Assets Security and Other Applications*. CRC Press, 2004. ISBN: 9780824750916

[2] LANGELAAR, G. C., SETYAWAN, I., LAGENDIJK, R. L. Watermarking digital image and video data. A state-of-the-art overview. *IEEE Signal Processing Magazine*, 2000, vol. 17, p. 20 to 46. DOI: 10.1109/79.879337

[3] WÓJTOWICZ, W., OGIELA, M. R. Digital images authentication scheme based on bimodal biometric watermarking in

an independent domain. *Journal of Visual Communication and Image Representation,* 2016, vol. 38, p. 1–10. DOI: 10.1016/j.jvcir.2016.02.006

[4] RABIZADEH, M., AMIRMAZLAGHANI, M., AHMADIAN-ATTARI, M. A new detector for contourlet domain multiplicative image watermarking using Bessel K form distribution. *Journal of Visual Communication and Image Representation*, 2016, vol. 40, Part A, p. 324–334. DOI: 10.1016/j.jvcir.2016.07.001

[5] BUM-SOO, K., CHOI, J. G., PARK, C. H., et al. Robust digital image watermarking method against geometrical attacks. *Real-Time Imaging*, 2003, vol. 9, p. 139–149. DOI: 10.1016/s1077-2014(03)00020-2

[6] NAJIH, A., AL-HADDAD, S.A.R., RAMLI, A. R., et al. Digital image watermarking based on angle quantization in discrete contourlet transform. *Journal of King Saud University - Computer and Information Sciences*. [Online] Cited April 4, 2016. DOI: 10.1016/j.jksuci.2016.02.005

[7] XIANG-YANG WANG, AI-LONG WANG, HONG-JING YANG, et al. A new robust digital watermarking based on exponent moments invariants in nonsubsampled contourlet transform domain. *Computers & Electrical Engineering*, April 2014, vol. 40, no. 3, p. 942–955. DOI: 10.1016/j.compeleceng.2013.12.017

[8] CHAREYRON, G., DA RUGNA, J., TRÉMEAU, A. Chapter 3: Color in Image Watermarking. *Advanced Techniques in Multimedia Watermarking: Image, Video and Audio Applications*. IGI Global Press, p. 36–56, 2010. ISBN: 1615209042

[9] TRÉMEAU, A., TOMINAGA, S., PLATANIOTIS, K. Color in image and video processing: Most recent trends and future research directions. *EURASIP Journal on Image and Video Processing*, 2008. DOI: 10.1155/2008/581371

[10] CHEMAK, C., LAPAYRE J. C., BOUHLEL, M. S. New watermarking scheme for security and transmission of medical images for pocket neuro project. *Radioengineering*, 2007, vol. 16, no. 4, p. 58–63. ISSN 1210-2512

[11] KUO-CHENG, L. Wavelet-based watermarking for color images through visual masking. *AEU - International Journal of Electronics and Communications*, 2010, vol. 64, no. 2, p. 112–124. DOI: 10.1016/j.aeue.2008.11.006

[12] CEDILLO-HERNANDEZ, M., CEDILLO-HERNANDEZ, A., GARCIA-UGALDE, F., NAKANO-MIYATAKE, M., PEREZ-MEANA, H. Copyright protection of color imaging using robust-encoded watermarking. *Radioengineering*, 2015, vol. 24, no. 1, p. 240–251. DOI: 10.13164/re.2015.0240

[13] BATTIATO, S., CATALANO, D., GALLO, G., GENNARO, R. Robust watermarking for images based on color manipulation. In *Proceedings of the Third International Workshop on Information Hiding*. Dresden (Germany), 1999. Springer-Verlag, 2000, vol. 1768, p. 302–317. DOI: 10.1007/10719724_21

[14] CHAREYRON, G., COLTUC, D., TREMEAU, A. Watermarking and authentication of color images based on segmentation of the XYZ color space. *Journal of Imaging Science and Technology*, 2006, vol. 50, no. 5, p. 411–423. DOI: 10.2352/J.ImagingSci.Technol.(2006)50:5(411)

[15] JIA, X., QI, Y., SHAO, L., JIA, X. An anti-geometric digital watermark algorithm based on histogram grouping and fault-tolerance channel. *Intelligent Science and Intelligent Data Engineering. Lecture Notes in Computer Science*, 2012, vol. 7202, p. 753–760. DOI: 10.1007/978-3-642-31919-8_96

[16] CHRYSOCHOS, E., FOTOPOULOS, V., XENOS, M., SKODRAS, A. N. Hybrid watermarking based on chaos and histogram modification. *Signal, Image and Video Processing*, 2014, vol. 8, no.5, p. 843–857. DOI 10.1007/s11760-012-0307-3

[17] CEDILLO-HERNANDEZ, M., GARCIA-UGALDE, F., NAKANO-MIYATAKE, M., PEREZ-MEANA H. Robust hybrid color image watermarking method based on DFT domain and 2D histogram modification. *Signal, Image and Video Processing*, 2014, vol. 8, no. 1, p. 49–63. DOI: 10.1007/s11760-013-0459-9

[18] SHAO-LI JIA. A novel blind color images watermarking based on SVD. *Optik - International Journal for Light and Electron Optics*, 2014, vol. 125, no. 12, p. 2868–2874. DOI: 10.1016/j.ijleo.2014.01.002

[19] LAUR, L., RASTI, P., AGOYI, M., ANBARJAFARI, G. A robust color image watermarking scheme using entropy and QR decomposition. *Radioengineering*, 2015, vol. 24, no. 4, p. 1025 to 1032. DOI: 10.13164/re.2015.1025

[20] PAN-PAN NIU, XIANG-YANG WANG, YI-PING YANG, MING-YU LU. A novel color image watermarking scheme in nonsampled contourlet-domain. *Expert Systems with Applications*, 2011, vol. 38, no. 3, p. 2081–2098. DOI: 10.1016/j.eswa.2010.07.147

[21] PRATHAP, I., NATARAJAN, V., ANITHA, R. Hybrid robust watermarking for color images. *Computers & Electrical Engineering*, 2014, vol. 40, no. 3, p. 920–930. DOI: 10.1016/j.compeleceng.2014.01.006

[22] DO, M. N., VETTERLI, M. The Contourlet transform: an efficient directional multiresolution image representation. *IEEE Transactions on Image Processing*, 2005, vol. 14, no. 12, p. 2091 to 2106. DOI: 10.1109/TIP.2005.859376

[23] MALVAR, H., FLORÊNCIO, D. Improved spread spectrum: a new modulation technique for robust watermarking. *IEEE Transactions on Image Processing*, 2003, vol. 51, no. 4, p. 898 to 905. DOI: 10.1109/TSP.2003.809385

[24] JIMENEZ-SALINAS, M., GARCIA-UGALDE, F. Improved spread spectrum image watermarking in contourlet domain. In *2008 23rd International Conference Image and Vision Computing.* Christchurch (New Zealand), 2008, 6 p. DOI: 10.1109/IVCNZ.2008.4762090

[25] SHEIKH, H. R., BOVIK, A. C. Image information and visual quality. *IEEE Transactions on Image Processing*, 2006, vol. 15, no. 2, p. 430–444. DOI: 10.1109/TIP.2005.859378

[26] WANG, Z., BOVIK, A. C., SHEIKH, H. R., SIMONCELLI, E. P. Image quality assessment: From error measurement to structural similarity. *IEEE Transactions on Image Processing*, 2004, vol. 13, no. 4, p. 600–612. DOI: 10.1109/TIP.2003.819861

[27] CHANG, H., CHEN, H. H. Stochastic color interpolation for digital cameras. *IEEE Transactions on Circuits and Systems for Video Technology*, 2007, vol. 17, no. 8, p. 964–973. DOI: 10.1109/TCSVT.2007.897471

[28] CAYRE, F., FONTAINE, C., FURON, T. Watermarking security: theory and practice. *IEEE Transactions on Signal Processing*, 2005, vol. 53, no. 10, p. 3976–3987. DOI: 10.1109/TSP.2005.855418

[29] CEDILLO-HERNANDEZ, M., GARCIA-UGALDE, F., NAKANO-MIYATAKE, M., PEREZ-MEANA, H. Robust object-based watermarking using SURF feature matching and DFT domain. *Radioengineering*, 2013, vol. 22, no. 4, p. 1057–1071. ISSN 1210-2512

[30] PROAKIS, J. G., SALEHI, M. *Digital Communications.* 5th ed. McGraw-Hill, 2008. p. 336, 351, 361. ISB: 0072321113

[31] KALKER, T. Considerations on watermarking security. In *Proceedings of 2001 IEEE Fourth Workshop on Multimedia Signal Processing MMSP*. Cannes (France), 2001, p. 201–206. DOI: 10.1109/MMSP.2001.962734

About the Authors ...

Manuel CEDILLO-HERNANDEZ was born in Mexico. He received the B.S. degree in Computer Engineering, M.S. degree in Microelectronics Engineering and his Ph.D. in Communications and Electronic in the National Polytechnic Institute of Mexico (IPN) in 2003, 2006 and 2011, respectively. Currently, he is a full-time researcher at Seccion de Estudios de Posgrado e Investigacion of ESIME Culhuacan in the Instituto Politecnico Nacional de Mexico. His principal research interests are image and video processing, watermarking, software development and related fields.

Antonio CEDILLO-HERNANDEZ was born in Mexico. He received the B.S. degree in Computer Engineering, M.S. degree in Microelectronics Engineering and his Ph.D. in Communications and Electronic in IPN in 2005, 2007 and 2013, respectively. His principal research interests are video processing, watermarking, software development and related fields.

Francisco GARCIA-UGALDE was born in Mexico. He obtained his bachelor in 1977 in Electronics and Electrical System Engineering from National Autonomous University of Mexico, his Diplôme d'Ingénieur in 1980 from SUPELEC France, and his Ph.D. in 1982 in Information Processing from Université de Rennes I, France. Since 1983 is a full-time professor at UNAM, Engineering Faculty. His current interest fields are: Image and video coding, image analysis, watermarking, theory and applications of error control coding, turbo coding, and applications of cryptography, parallel processing and data bases.

Mariko NAKANO-MIYATAKE was born in Japan. She received the M.E. degree in Electrical Engineering from the University of Electro-Communications, Tokyo, Japan in 1985, and her Ph.D. in Electrical Engineering from The Universidad Autonoma Metropolitana (UAM), Mexico City, in 1998. In February 1997, she joined the Graduate Department of The Mechanical and Electrical Engineering School, IPN, where she is now a Professor. Her research interests are in information security, image processing, pattern recognition and related field.

Hector PEREZ-MEANA was born in Mexico. He received his M.S. Degree in Electrical Engineering from the Electro-Communications University of Tokyo, Japan in 1986 and his Ph.D. degree in Electrical Engineering from the Tokyo Institute of Technology, Tokyo, Japan, in 1989. In February 1997, he joined the Graduate Studies and Research Section of The Mechanical and Electrical Engineering School, IPN, where he is now a Professor. His principal research interests are adaptive systems, image processing, pattern recognition, watermarking and related fields.